EPJ Web of Conferences **26**, 04030 (2012)
DOI: 10.1051/epjconf/20122604030

Polymer behaviour and fracture models in dynamic

R. Balieu[1,2,3,a], F. Lauro[1,2,3], B. Bennani[1,2,3], B. Bourel[1,2,3], and K. Nakaya[4]

[1] *Univ. Lille Nord de France, 59000 Lille, France*
[2] *UVHC, LAMIH, 59313 Valenciennes, France*
[3] *CNRS, UNR 8201, 59313 Valenciennes, France*
[4] *TOYOTA MOTOR EUROPE, 1140 Brussels, Belgium*

Abstract. A phenomenological small strain model is developed to capture the elastoviscoplastic behaviour of a 20% filled polypropylene. The constitutive model is based on a multiplicative viscoplastic law. The hydrostatic pressure dependency is considered by using the Drucker Prager yield surface. A phenomenological damage model characterised directly by experimental investigation is used to capture the yield degradation during the deformation in tension. The volume variation due to the cavitation phenomenon is captured by using non-associated viscoplasticity. Some experimental tests at different speed loadings are carried out for the parameters identification of the constitutive model. Furthermore, a fracture model which depends on the stress triaxiality and the strain rate is developed in order to model the complete behaviour of the material studied until fracture.

1 Introduction

Semi-crystalline polymers are widely used for structural applications in the automotive sector. Their complex mechanical behaviour due to the important number of dependent parameters (temperature, humidity, strain rate and stress triaxiality) has been largely investigated since many years in the literature. Two approaches are usually used to capture the complex behaviour of solid polymers. A physical assumption, widely used for amorphous polymer, where the constitutive equations are based on the macromolecular structure and the affine network [1,2]. In other way, some phenomenological approaches based on viscoplastic models, initially developed for metals and theirs alloys, can be used to capture the elastoviscoplastic behaviour of polymers. The viscoplastic models based on overstress (VBO) was adopted by Ho and Krempl [3] and Krempl and Khan [4] to describe the inelastic behaviour of polymers. The phenomenological VBO models are able to describe the strain rate influence of some polymers in uniaxial loading case but depends only on the second invariant of the deviatoric stress tensor. In the particular case of filled polymer, the well-known cavitation phenomenon due to the decohesion at charge-matrix interface occurs. In this case, the elastoviscoplastic response is associated to damage in the form of nucleation, growth and coalescence of cavities. For these kinds of materials, the assumption of constant inelastic volume during the deformation is not acceptable. The main objective of this work is the development of a phenomenological constitutive model able to capture the elastoviscoplastic behaviour of a 20% filled polypropylene on a large range of strain rates under different loadings. A constitutive model based on the non-associated viscoplastic theory is used to model the volume variation and the viscous effect. The Drucker Prager pressure dependent yield surface [5], initially employed for soils modelling is used in the viscoplastic flow in order to take the hydrostatic pressure into account. A damage model which depends on the equivalent plastic strain is introduced in the yield function to represent the softening effect observed in uniaxial tensile loading. The material parameters of the constitutive model are identified from experimental tests at different speed loadings. The viscous behaviour law is deduced by using the SEÈ method [6]. With this measurement technique, the behaviour laws at constant strain rate are deduced on a large strain rate range (quasi-static and dynamic).

As the behaviour of semi-crystalline polymers, the fracture of these materials is known to be very complex. A first proposal was done by Morin et al. [7] for an epoxy material. In this paper, a fracture model is developed to take the stress triaxiality and the strain rate into account. The constitutive fracture model is a modification of the Xue-Wierzbicki model [8] which depends on the stress triaxiality and the Lode parameter. The modification consists on the introduction of a non linear strain rate effect. With this fracture model a fracture surface is therefore obtained in order to capture the fracture of the material studied for a large range of stress triaxiality and strain rates.

2 Constitutive behaviour model

A non-symmetric yield surface is used to represent the behaviour of the polymer in tension and compression loading. The yield surface introduced by Drucker and Prager is used to model this non-symmetry. This yield surface considers that the plasticity occurs when the von Mises equivalent stress and the hydrostatic pressure reach a critical combination. The yield surface of the constitutive model is given by

$$f(\underset{\sim}{\sigma}, D, \kappa) = \frac{\sqrt{3J_2\left(\underset{\sim}{\mathbf{S}}\right)} + \eta p}{1 - D} - \xi\sigma_y(\kappa). \qquad (1)$$

[a] e-mail: romain.balieu@univ-valenciennes.fr

where $\underset{\sim}{\sigma}$ is the stress tensor, J_2 is the second invariant of the deviatoric stress tensor defined by

$$J_2 = \frac{1}{2}\underset{\sim}{\mathbf{S}} : \underset{\sim}{\mathbf{S}}. \tag{2}$$

The symbol (:) represents the doubly contracted product tensor and $\underset{\sim}{\mathbf{S}}$ is the deviatoric stress tensor given by

$$\underset{\sim}{\mathbf{S}} = \underset{\sim}{\sigma} - p\,\underset{\sim}{\mathbf{I}}. \tag{3}$$

$\underset{\sim}{\mathbf{I}}$ is the second order unity tensor and p the hydrostatic pressure such as

$$\underset{\sim}{\mathbf{S}} = \frac{1}{3}\mathrm{tr}(p), \tag{4}$$

where tr(.) is the trace of a second order tensor. The behaviour law σ_y under tensile loading depends on the equivalent plastic strain κ. By following the viscoplastic theory, the equivalent plastic strain is given by

$$\kappa = \sqrt{\tfrac{2}{3}\,\underset{\sim}{\varepsilon}^{\mathrm{vp}} : \underset{\sim}{\varepsilon}^{\mathrm{vp}}}, \tag{5}$$

where $\underset{\sim}{\varepsilon}^{\mathrm{vp}}$ is the viscoplastic strain tensor. The material parameters η and ξ , which characterise the hydrostatic pressure dependency are defined by the ratio between the yield stresses in tension and compression, respectively σ_t and σ_c, such as

$$\eta = 3\frac{\sigma_c/\sigma_t - 1}{\sigma_c/\sigma_t + 1} \quad \text{and} \quad \xi = 1 + \frac{\eta}{3}. \tag{6}$$

As in the classical small strain viscoplastic theory, the total strain rate tensor $\underset{\sim}{\varepsilon}$ is additively decomposed into an elastic component $\underset{\sim}{\varepsilon}^{\mathrm{e}}$ and a viscoplastic component $\underset{\sim}{\varepsilon}^{\mathrm{vp}}$ such as

$$\underset{\sim}{\varepsilon} = \underset{\sim}{\varepsilon}^{\mathrm{e}} + \underset{\sim}{\varepsilon}^{\mathrm{vp}}. \tag{7}$$

The viscoplastic strain rate tensor evolves with the flow rule, as follows

$$\dot{\underset{\sim}{\varepsilon}}^{\mathrm{vp}} = \dot{\gamma}\,\underset{\sim}{\mathbf{n}}. \tag{8}$$

$\dot{\gamma}$ is the rate form of the plastic multiplier $\Delta\gamma$. The plastic deformation of the polymer studied is not an isochoric phenomenon. The non-associated viscoplasticity is therefore used to represent this volume variation. In the constitutive model, the flow rule, $\underset{\sim}{\mathbf{n}}$ is derived from a plastic potential g such as

$$\underset{\sim}{\mathbf{n}} = \frac{\partial g}{\partial \underset{\sim}{\sigma}}. \tag{9}$$

The plastic potential g is different to the yield surface due to the non-associated viscoplasticity. The plastic potential of the constitutive model is defined by

$$g\left(\underset{\sim}{\sigma}\right) = \frac{\sqrt{3J_2\left(\underset{\sim}{\mathbf{S}}\right)} + \alpha p}{1 - D}. \tag{10}$$

The parameter α depends on the plastic Poisson ratio ν_p as

$$\nu_p = a\ \exp(b\,h\,\kappa) + c, \tag{11}$$

where the scalars a, b and c are deduced experimentally. The parameter h is introduced to take the stress triaxiality influence on the volume variation into account. h is defined as follows

$$h = \begin{cases} h = 1 & \text{if } p > 0, \\ h = 0 & \text{if } p \le 0. \end{cases} \tag{12}$$

The plastic Poisson ratio ν_p is defined by

$$\nu_p = -\frac{\varepsilon_{22}}{\varepsilon_{11}}, \tag{13}$$

where ε_{22} and ε_{11} are respectively the transverse and longitudinal strain components. In the constitutive model, the strain rate tensor, which directly uses the strain rate parameter determined experimentally, is given by

$$\dot{\underset{\sim}{\varepsilon}}^{vp} = \frac{\dot{\kappa}_0}{\sqrt{\frac{2}{3}\underset{\sim}{\mathbf{n}} : \underset{\sim}{\mathbf{n}}}}\left(\frac{\sqrt{3J_2} + \eta p}{\xi(1-D)\sigma_y}\right)^{1/n}\underset{\sim}{\mathbf{n}}. \tag{14}$$

The parameter n, κ_0 and the static behaviour law σ_y are deduced directly from experimental data from different uniaxial tensile tests carried out at different strain rates.

The damage model used in the the yield surface (Eq. (1)) and the plastic potential (Eq. 10) is purely phenomenological. This model is based on stress difference between the isochoric and non-isochoric deformation process. This damage model is a ratio between the true stress calculated with the incompressibilty and compressibility assumption. The damage model is a function of the equivalent plastic strain κ given by

$$D = \begin{cases} 1 - \omega(\kappa) & \text{if } \omega(\kappa) \le 1, \\ 1 & \text{if } \omega(\kappa) > 1, \end{cases} \tag{15}$$

where function $\omega(\kappa)$ is given by

$$\omega(\kappa) = 1 - \exp\left(-\frac{\kappa}{k_c}\right). \tag{16}$$

k_c is a material parameter deduced from experimental tests.

3 Identification of the material parameters and results

The damage function, the plastic Poisson ratio (not constant) and the behaviour law are deduced directly from the experimental tests by using the SEÈ method [6]. The SEÈ method was developed by the authors to perform the true behaviour laws in uniaxial tensile loading at constant strain rate for a large range of strain rates (quasi-static and dynamic). By using the Digital Image Correlation (DIC) measurement, the true stress-strain behaviour laws of the material are calculated for different speed loadings. By combining with the true strain rate (not constant) measured by DIC as well, it results a true behaviour surface. By cutting this behaviour surface at the desired strain rate, the behaviour laws at constant strain rate are therefore obtained. For the uniaxial tensile tests, the 2D Digital Image Correlation is therefore employed for the strain field measurements with high speed camera (PHOTRON APX 3000). The Digital Image Correlation measures the displacement field on the surface of the specimen between

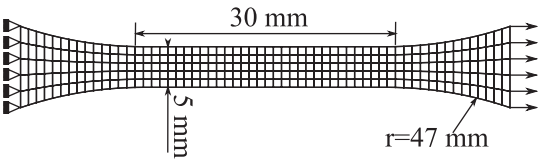

Fig. 1. Boundary conditions and finite element mesh of the uniaxial tensile tests.

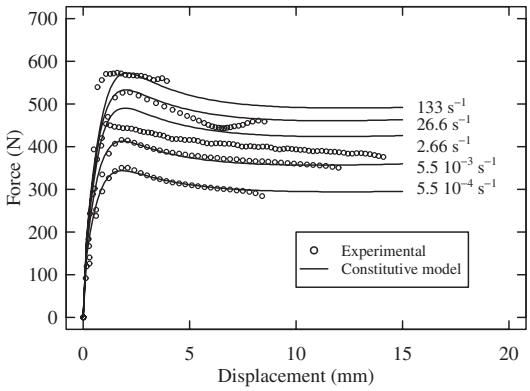

Fig. 2. Experimental vs constitutive model in uniaxial tensile loading.

two pictures, by using an artificial texture obtained by painting the surface of the specimen with black and white colors in order to obtain different grey scale levels. The uniaxial tensile tests are carried out on an electromagnetic device (INSTRON E3000) for the quasi-static cases with a 3 kN cell force. A hydraulic high speed device (INSTRON 65/20) is used for the dynamic loadings with a 5 kN cell force, at room temperature. The quasi-static compression tests are performed on the electromagnetic device (INSTRON E3000) and the hydraulic high speed device (INSTRON 65/20) is used for the dynamic tests. The displacements are measured with an optical extensometer (Rudolph 200XR).

The numerical uniaxial tensile tests presented in this section are carried out at 5 loading speeds: 1 mm/s 100 mm/s 0.08 m/s, 0.8 m/s and 4 m/s which correspond to an approximate equivalent strain rate of respectively 5.5 10^{-4}, 5.5 10^{-2}, 2.6, 26.6 and 133 s^{-1}. The geometry of the specimen, boundary conditions and finite elements mesh are shown in Fig. 1. For the simulation, the specimen is meshed with fully integrated shell elements and 3 integration points in the thickness. The comparison between the constitutive model and the experimental data is shown in Fig. 2. The reaction forces on the middle of specimens as function of the displacements enforced at the right boundaries are confronted to the experimental data. The constitutive model is in good agreement with the experimental measurements for all the speed loadings.

The numerical uniaxial compression tests are carried out at 3 loading speeds: 1 mm/min, 1 mm/s and 150 mm/s which correspond to an approximate equivalent strain rate of respectively 5.2 10^{-3}, 0.3 and 46 s^{-1}. The cylinder used to simulate the uniaxial compression tests is modelled with fully integrated height node hexahedral elements. For a more efficient solution, the analysis is performed on a quarter of the section with appropriate boundary

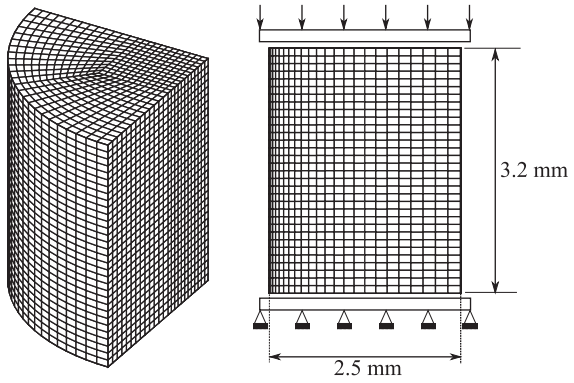

Fig. 3. Finite element mesh and boundary conditions for uniaxial compression tests.

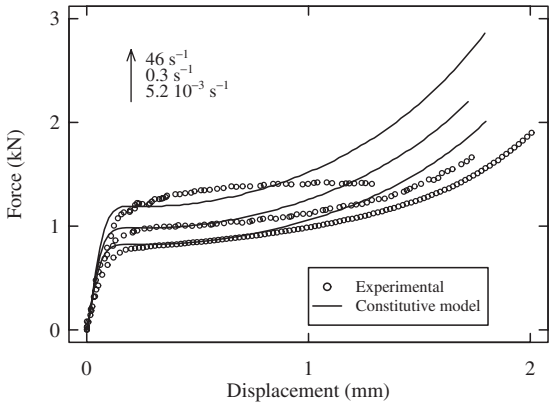

Fig. 4. Experimental versus constitutive model in uniaxial compression loading.

conditions (2 symmetries). The analysis is carried out with two rigid bodies. The loading consists of a prescribed monotonic velocity (with free vertical displacement) imposed on the rigid body placed on the top of the specimen. The other rigid body (at the bottom of the specimen) has its displacement following the loading direction clamped. The two rigid bodies are also in contact with the specimen with a friction coefficient of 0.05. The geometry of the specimen, boundary conditions and finite element mesh are shown in Fig. 3. The correlation between the numerical simulation and the experimental tests in uniaxial compression loading is shown in Fig. 4. The reaction force versus the displacement of the top of the specimen is compared with the experimental tests. The strain rate effect on the yield stress is well captured. The constitutive model has a good correlation in terms of hardening evolution for low deformation ($\kappa \leq 20\%$) but the numerical responses move away from the experimental data for higher deformation.

Due to the non-localisation of the deformation in a small part of the specimen in uniaxial tensile loading, the comparison of the true local strain components can not be made with the uniaxial tensile test. In order to compare the true strain components of numerical response with the real strain evolution, an experimental uniaxial tensile test is carried out on a notched tensile specimen. The experimental tensile test is performed on the hydraulic high speed device (INSTRON 65/20) at 0.08 m/s. As in uniaxial tensile tests, the Digital Image Correlation is

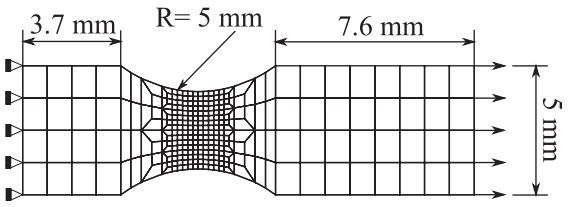

Fig. 5. Finite element mesh and boundary conditions for notched tensile tests.

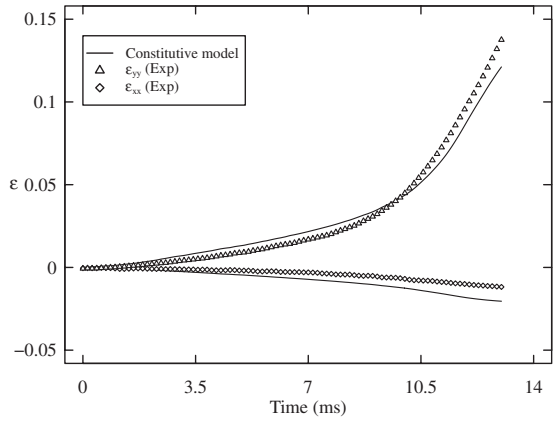

Fig. 6. True local strain comparison between the constitutive model and the experimental test.

used for the local strain measurements. The simulation of the tensile test with the notched specimen is performed with the constitutive model. Geometries and boundary conditions of the specimen are given in Fig. 5. For this simulation, a prescribed relative displacement measured directly by the Digital Image Correlation is applied to the right of the specimens. In order to compare the true strains of the numerical model with the experimental test, the size of ZOI (Zone of Interest) used in the digital image software VIC 2D® is the same as the finite element mesh in the center of the specimens (0.2 mm). Fig. 6 shows the true strains correlation between the constitutive model and the experimental test. The true strain comparison is made on the element (ZOI in digital image correlation measurement) in the center of the specimen where the longitudinal strain is higher. The numerical results in terms of local strains (longitudinal and transverse) are very close to the experimental ones. The model is also able to describe the volume variation of the material observed experimentally.

4 Fracture characterisation and physical interpretations

Experimental tests carried out at different speeds and loadings highlight the stress triaxiality and the strain rate influence on the fracture of the polymer studied. The tensile tests and notched tensile tests performed in quasi-static and dynamic with Digital Image Correlation are used to extract the equivalent fracture strain ε_f for different loadings and at different strain rates. Two notched specimens are tested to obtain the fracture strain values for

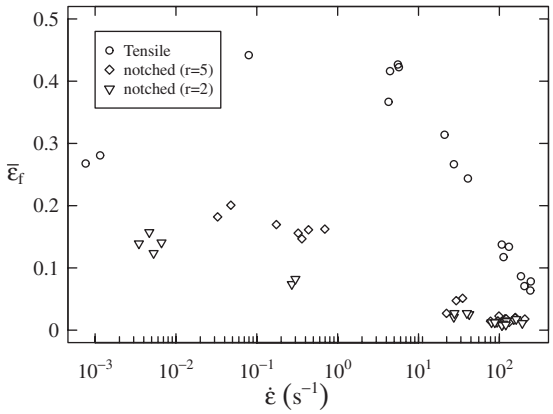

Fig. 7. Equivalent fracture strain for tensile and notched tensile specimens.

stress triaxiality parameter higher than the tensile state. The notched tensile specimen geometries are based on the classical tensile geometry with simply a half hole (r = 2 and 5 mm) on each side of the specimen. Compression tests are carried out too and its results that no fracture occurs in compression loading for all the speed loadings. For all the tests, the fracture strain is measured on the picture where the crack appears. The fracture strain is calculated as an equivalent strain as follows

$$\varepsilon_f = \sqrt{\tfrac{2}{3}\underset{\sim}{\varepsilon}:\underset{\sim}{\varepsilon}}. \tag{17}$$

The fracture strain rate is calculated with the above fracture strain $\varepsilon_f(t)$ and the equivalent strain of the previous picture $\varepsilon_f(t - \Delta t)$ by the following relation

$$\dot{\varepsilon}_f = \frac{\varepsilon_f(t) - \varepsilon_f(t - \Delta t)}{\Delta t}, \tag{18}$$

where Δt is the time between two pictures. Fig. 7 shows the stress triaxiality and the strain rate influence on the fracture strain of the tensile and notched tensile specimens. For the tensile tests an increase of the fracture strain versus strain rate is observed for low strain rates. This increase is probably due to the temperature effect. Next, for strain rates higher than $10^{-1}\,s^{-1}$, a decrease of the fracture strain when the strain rate increases is observed. The results of the notched tensile tests does not have the same tendency, a decrease of the fracture strain when the strain rate increases is observed for all the tests. The obvious stress triaxiality dependency is clearly highlighted by these results, a decrease of the fracture strain when the stress triaxiality parameter increases (on the range 0.33–0.5) is observed for the same strain rate.

The irregular strain rate influence on the tensile tests in term of fracture can be explained by the cavitation phenomenon. The material being studied is a mineral filled polypropylene where the decohesion at charge-matrix interface occurs. In this case the elastoviscoplastic response is associated to damage in the form of nucleation, growth and coalescence of cavities. Fig. 8 shows the fracture facies for the tensile test in quasi-static for an approximate strain rate of $10^{-3}\,s^{-1}$. The fracture facies shows lot of cavities and an important decohesion between the charges and the

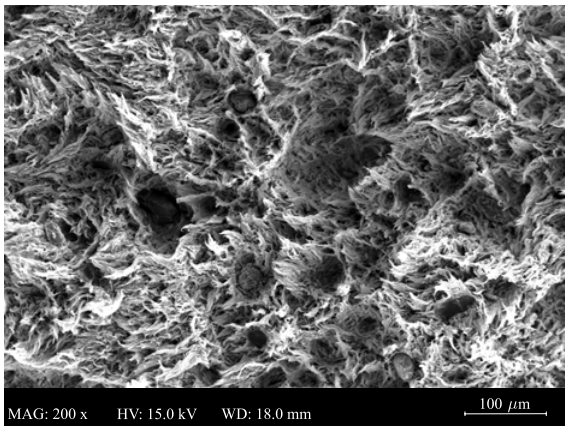

Fig. 8. Fracture facies for the tensile specimens at 10^{-3} s^{-1}.

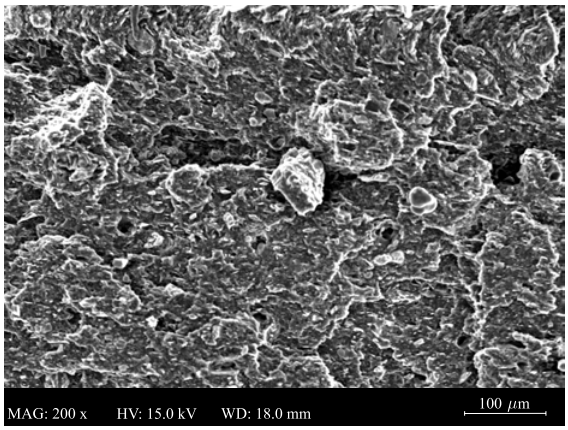

Fig. 9. Fracture facies for the tensile specimens at 300 s^{-1}.

matrix. Fig. 9 shows the fracture facies for the tensile test in dynamic for an approximate strain rate of 300 s^{-1}. This facies is very different as the above fracture. At this strain rate no decohesion at charge-matrix interface occurs. For relative low strain rate the cavitation phenomenon occurs and the value of fracture strain is relatively low due to the important number of cavities. When the strain rate increases sufficiently (around 10^{-1} s^{-1}) the decohesion at charge-matrix interface starts to decrease and the fracture strain value depends more on the strain rate (decreases when the strain rate increases). The cavitation phenomenon occurs for the notched tensile tests at low strain rates as well, however, the strong stress triaxiality influence shown in Fig. 6 makes not visible (at a macroscopic scale) this phenomenon on the global fracture strain value.

5 Constitutive fracture model

As shown is Section 4, the fracture model needs to depend on the stress triaxiality and the strain rate. The constitutive fracture model is based on the Xue-Wierzbicki model [8] which depends on the stress triaxiality and the Lode parameter. The Xue-Wierzbicki model is given by

$$\varepsilon_f = C_1 e^{(-C_2\upsilon)} - \left(C_1 e^{-C_2\upsilon} - C_3 e^{-C_4\upsilon}\right)\left(1-\zeta^{1/n}\right)^n, \quad (19)$$

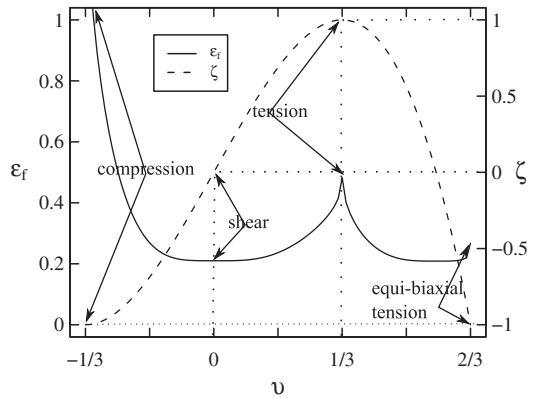

Fig. 10. Equivalent fracture strain given by Xue-Wierzbicki's model (solid line). Evolution of the Lode parameter (dashed line).

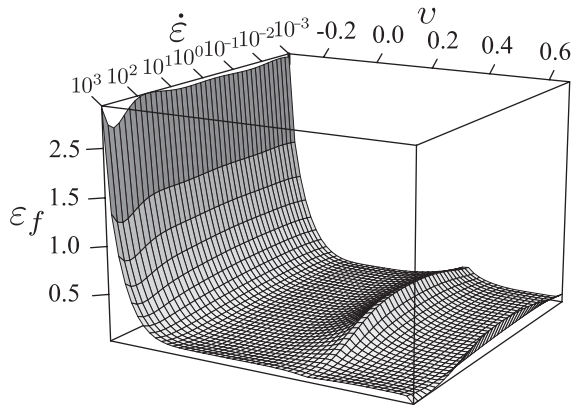

Fig. 11. Fracture surface given by the constitutive fracture model.

where C_1, C_2, C_3, C_4 and n are material parameters. υ is the stress triaxiality parameter such as

$$\upsilon = \frac{p}{\sqrt{3J_2(\tilde{\mathbf{S}})}}. \quad (20)$$

ζ is the Lode parameter which is function of the stress triaxiality parameter given by

$$\zeta = -\frac{27}{2}\upsilon^3 + \frac{9}{2}\upsilon. \quad (21)$$

The Lode parameter is another stress measurement which oscillates between -1 and 1. The aim of the Lode parameter is to increase the fracture strain in tension and compression loadings and to decrease this value in shear loading. Fig. 10 shows the equivalent fracture strain (solid line) given by the Xue-Wierzbicki model where the values of C_1, C_2, C_3, C_4 and n are respectively 0.87, 1.77, 0.21, 0.01 and $\frac{1}{4}$. On the same figure, the value of the Lode parameter for each stress triaxiality parameter is represented (dashed line).

The above fracture criterion was developed for 2024-T351 aluminum alloy where the fracture strain does not depend on the strain rate. The proposed fracture criterion is a modification of the Xue-Wierzbicki model in order to take the strain rate effect into account. The proposed fracture criterion is given by

$$\varepsilon_f = C_1(\dot{\varepsilon}) e^{(-C_2(\dot{\varepsilon})\upsilon)} - \left(C_1(\dot{\varepsilon}) e^{-C_2(\dot{\varepsilon})\upsilon} - C_3(\dot{\varepsilon})\right)\left(1-\zeta^{1/n}\right)^n. \quad (22)$$

$C1$, $C2$ and $C3$ are therefore function of the strain rate. To ensure the continuity of the model, the parameter n cannot be function of the strain rate. The functions $C1$, $C2$ and $C3$ are fitted with a sixth order polynomial function from experimental values of the fracture strain with an fixed stress triaxiality parameter. As shown in Fig. 11, the constitutive fracture model is therefore a fracture surface which depends on the stress triaxiality parameter and the strain rate.

6 Conclusions

A phenomenological elastoviscoplastic model is developed in this paper in order to simulate by finite element simulation the behaviour observed experimentally of a 20% mineral filled semi-crystalline polypropylene. The constitutive model is able to represent the non linear strain rate sensitivity by using a viscoplastic model developed from a multiplicative form of rate dependent behaviour law. The non-associated viscoplastic potential based on a non-constant plastic Poisson ratio is used in order to capture the volume change of the material being studied. The fully coupled damage model, which uses the concept of effective stress, is able to represent the softening behaviour which occurs after the hook observed experimentally. The introduction of the hydrostatic pressure for the description of the yield stress in the model allows one to model the kind of loading influence on the material behaviour.

A fracture model able to capture the non-linear strain rate effect and the stress triaxiality is developed by using a 3D mathematical model which depends on the strain rate and the stress triaxiality. This fracture model will be validate by comparing results of experimental bulge tests and finite element modelling. This constitutive model will be used to simulate industrial structures included in large finite element model.

Acknowledgements

The present research work has been supported by the International Campus on Safety and Intermodality in Transportation, the Nord-Pas-de-Calais Region, the European Community, the Regional Delegation for Research and Technology, the Ministry of Higher Education and Research, and the National Center for Scientific Research and TOYOTA MOTOR EUROPE.

References

1. Arruda, E.M., Boyce, M.C., Journal of the Mechanics and Physics of Solids **41**, (1993) 389-412
2. Ayoub, G., Zaïri, F., Naït-Abdelaziz, M., Gloaguen, Journal of Plasticity **26**, (1993) 329-347
3. Ho, K., Krempl, E., International Journal of Plasticity **18**, (2002) 851-872
4. Krempl, E., Khan, F., International Journal of Plasticity **19**, (2003) 1069-1095
5. Drucker, D., Prager, W., Quartely of Applied Mathematics **10**, (1952) 157-165
6. Lauro, F., Bennani, B., Morin, D., Epee, A., International Journal of Impact Engineering **37**, (2010) 715-722
7. Morin, D., Haugou, G., Bennani, B., Lauro, F., Engineering Fracture Mechanics **77**, (2010) 3481-3500
8. Wierzbicki, T., Bao, Y., Lee, Y.W., Bai, Y., International Journal of Mechanical Sciences **47**, (2005) 719-743